Chapter 6
State of the Art and Technical Trends

6.1 Introduction

This chapter presents the state of the art of the principal uncooled focal plane array technologies and the systems that employ them. All data are from current technical publications, rather than manufacturers' literature. Systems based on the three principal detection mechanisms are included (see Chapters 3, 4, and 5). The chapter concludes with a brief review of technical trends in the military and commercial markets for uncooled imagers and imaging radiometers.

6.2 Resistive Bolometer Arrays and Their Applications in Thermal Imagers and Imaging Radiometers

6.2.1 The Honeywell silicon microstructure resistive bolometer array and thermal imager

Most modern resistive bolometer array technology derives from the pioneering efforts of a team under the direction of R. Andrew Wood at the Honeywell Technology Center that began in 1982. The basis was the following:

- It had been realized for twenty years[1] that the key to bolometer performance was not the resistive material but the thermal isolation structure.
- Silicon micromachining technology, which was under development at Honeywell for low cost, low power sensors of various types, was an ideal technology for providing excellent thermal isolation structures.
- The U.S. Department of Defense, especially DARPA (Defense Advanced Research Projects Agency) and NVESD (U.S. Army Night Vision and Electronic Sensors Directorate) was a source of the many millions of dollars of funding and for technical guidance and military requirements definition, necessary for the full development of uncooled imaging array technology.

As a result, Honeywell Technology Center received military contracts beginning in 1985 which led to the successful development of an uncooled microbolometer array containing 336 columns × 240 rows of 50 × 50-μm pixels operating at the U.S. TV frame rate of 30 Hz.

The chosen resistive material was vanadium oxide, which was known to have a high temperature coefficient of resistance at room temperature and which was process compatible with silicon technology. It was deposited on a "microbridge" of silicon nitride (Si_3N_4) by ion beam sputtering, resulting in a mixture of several forms of vanadium oxide, symbolized by VOx. The properties of VOx are shown in Figs. 4-4 and 4-5. Currently, it remains the material of choice, with amorphous silicon emerging as a strong contender.

The original Honeywell approach employed a front-side anisotropic etchant (see Fig. 6-1). This required the electronics to be alongside the sensitive area, thereby reducing the pixel "fill factor," i.e., the fraction of the pixel area that responded to the incident radiation. To improve the fill factor, Honeywell developed a two-level structure (see Fig. 6-1), with the electronics buried in the silicon beneath the bridge. This was achieved through the deposition of a silicon oxide sacrificial layer, 2.5-μm thick, which was removed after the microbridge layer had been deposited, thereby leaving a 2.5-μm gap between the substrate and the microbridge. Figure 6-2 illustrates the process steps. A reflecting layer was deposited on the surface of the silicon below the microbridge. Radiation incident upon the microbridge, whose thickness was less than 1 μm, was not fully absorbed. That part that was transmitted was reflected by the mirror back to the microbridge. The choice of 2.5 μm as the distance from the microbridge to the mirror was driven by the desire to have a resonant optical cavity tuned to the middle of the 8–14-μm spectral interval, where the spectral emittance of the earth peaks and where there is an atmospheric window. In this manner, the optical absorption of the microbridge exceeded 80% throughout the 8–14-μm spectral interval.

A two-level structure requires electrical contacts from the upper level to the lower. This was achieved through "legs" (see Fig. 4-1). These legs reduce the fill factor. On the other hand, they determine the thermal conductance G, and therefore the thermal response time for a given pixel size with a standard microbridge thickness, therefore with a standard heat capacity C.

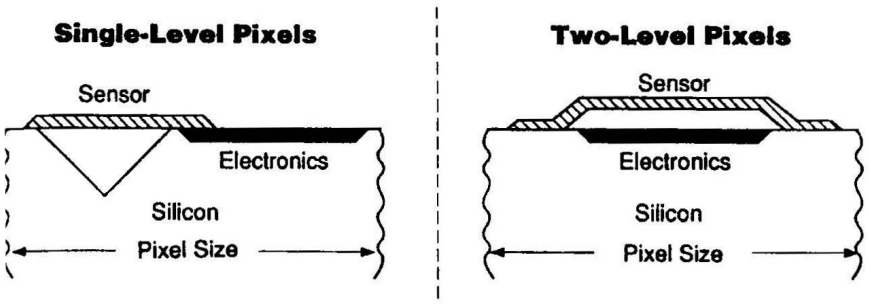

Figure 6-1. Illustration of one-level and two-level microbolometer designs. From R.A. Wood.[3]

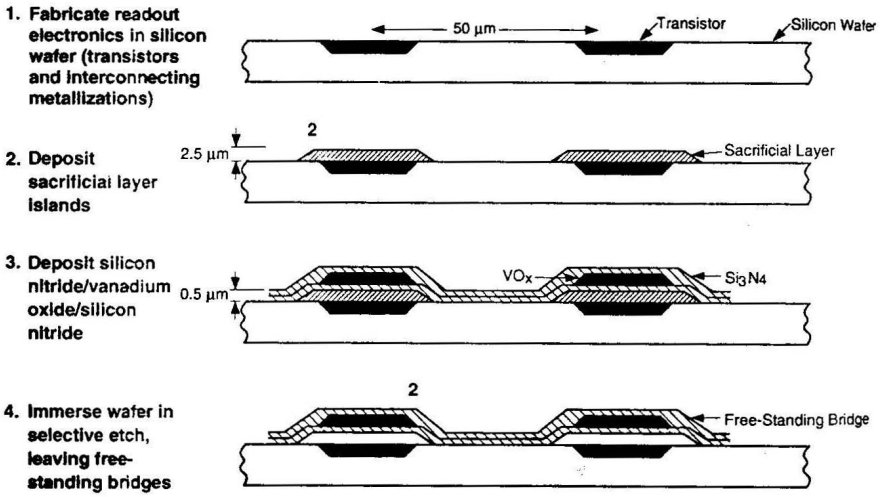

Figure 6-2. Fabrication sequence for two-level microbolometers. From R.A. Wood.[3]

Another issue that was faced by Honeywell was the need to read out the signal by accessing the pixels sequentially. The method chosen was by pulsing the electrical bias to the pixels sequentially, as described in Sec. 4.2.3 of Chapter 4. The switching was accomplished by implanting a bipolar transistor underneath each pixel. When a bias voltage was applied for about 100 μsec between a given row and column, only that pixel was switched to an "on" state. Bipolar transistors were the best solution to the switching problem given the design rules in place at Honeywell during the late 1980s. Today, CMOS (complementary metal oxide semiconductor) circuits are the usual choice, including at Honeywell.

There were two problems with the switching. First, the pulse current was required to be so high during the pulse that the pixel temperature rose several degrees C during the 100 μsec pulse duration (see Fig. 4-3). On top of that pulse rode the signal, which was of the order of a few thousandths of a degree centigrade. That pulse bias temperature rise had to be subtracted from the total rise to leave only the signal. Nonuniformity in resistance from pixel to pixel required the subtracted amount to vary from pixel to pixel. Furthermore, the radiation falling on the pixel originated not only through the lens but also from the interior of the vacuum package in which the array was mounted. The approach to this problem was to employ a temperature stabilizer upon which the array was mounted within a vacuum package (Fig. 6-3).

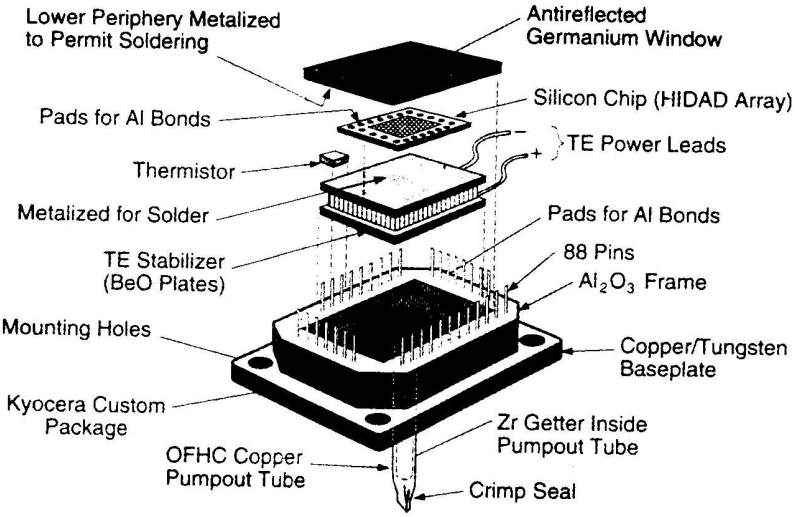

Figure 6-3. Construction of a sealed vacuum package for 240 × 336 microbolometer arrays. From R.A. Wood.[3]

The second problem with the switching had to do with the dynamic range and cycle speed of analog-to-digital (ADC) converters available in the late 1980s. In order to correct for pixel nonuniformities and to have a large dynamic range, a 14-bit ADC was required. The cycle speed of those available at the time would not allow 332 × 240, or 80,640, pixels to be digitized 30 times a second. Accordingly, the array was divided into 12 column groups, with 12 parallel outputs, which were then combined into a single frame. Figure 6-4 is a block diagram of the Honeywell imager. The iris is momentarily closed automatically as the focal plane array temperature drifts, so as to renormalize the pixel signals. When the original classified contracts under which the microbolometer was developed became declassified in 1992, Honeywell revealed the details of the development.[2] Subsequently there have been several Honeywell papers, see, for example, the chapter by Wood.[3] The performance at that time is summarized in Fig. 6-5 and Table 6-1.

It is instructive to compare the data of Table 6-1 with the temperature fluctuation noise calculation of Eq. (2.29), plotted in Fig. 2-3. Using the values listed, the temperature fluctuation noise limited NETD [see Eq. (2.29)] is 0.0052°C. The histogram, Fig. 6-5, shows that the mean NETD is 7.5 times that, although the best pixels are only about 5 times that. (All the NETD measurements reported in this chapter and others are for 300 K blackbody sources, *f*/1 optics, and 30-Hz bandwidth unless otherwise specified.)

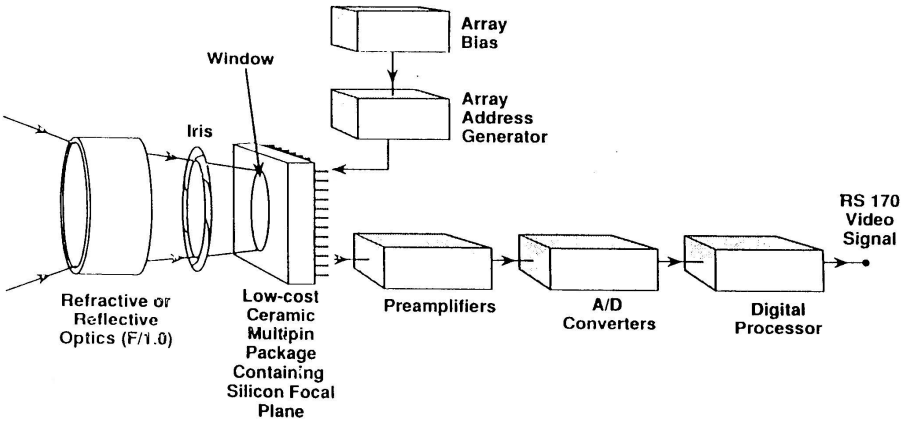

Figure 6-4. Block diagram of Honeywell uncooled bolometer imager. From R. A. Wood.[3]

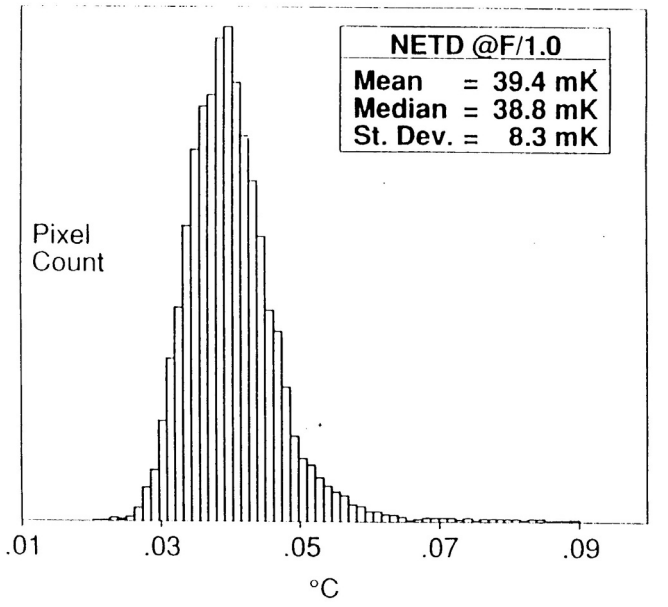

Figure 6-5. Measured NETD of 240 × 336 two-level microbolometer arrays of Table 6-1. From R.A. Wood.[3]

Table 6-1. Summary of 240 × 336 two-level microbolometer array parameters. From R.A. Wood.[3]

Parameter	Value
Array size	240 × 336
Pixel size	50 μm
Design	Two layer
Bridge	35 × 35 × 0.8 μm Si_3N_4
Legs	50 × 2 × 0.8 μm Si_3N_4
Fill factor	0.70
Package	Vacuum
Thermal stabilization	Thermoelectric stabilizer
Nominal operating temperature	25°C
Thermal capacity	$3 \times 10^{!9}$ J/deg K
Thermal conductance	$2 \times 10^{!7}$ W/deg K (in vacuum)
Time constant	15 msec (in vacuum)
Absorptance	80% mean, 8–14 μm
TCR material	500 Å VOx, TCR = !0.023 $(\text{deg K})^{!1}$
Pixel resistance	20 KΩ
Readout	Pulsed constant-voltage, bipolar transistor under each pixel, 14 pixels in parallel, 14 bipolar preamplifiers
Field rate	30 Hz
Frame rate	30 Hz
Offset compensation	Intermittent shutter
Bias	5 μsec 250 μA pulses
NETD	0.039°C, *f*/1, 8–14 μm, 300 K target

When the uncooled bolometer effort began at the Honeywell Technology Center, Honeywell Inc. owned a division that developed and manufactured infrared systems. That division was to have been the recipient of the uncooled technology developed at the Center. However, Honeywell sold that division and the Technology Center decided to license the technology. There were originally four licensees. Following acquisitions and mergers within the defense and aerospace industries, there are now three: British Aerospace (the original Honeywell division), Raytheon, and Boeing, with other licenses pending. The

technology advances made by these corporations and others worldwide, including the Honeywell Technology Center, are described below.

6.2.2 Improvements on the Honeywell VOx 240 × 332 pixel bolometer array

Currently there remains a great deal of activity on VOx bolometer arrays having a modified Honeywell microbolometer support structure. The improvements fall into the following categories.

6.2.2.1 Increase in fill factor

The Honeywell microbridge employed two supporting legs for electrical contact and thermal isolation. The pixel area taken up by the legs reduced the fill factor. Efforts to increase the fill factor include reducing the size of the contacts ("posts") and use of "buried" legs[4] on an intermediate level between the level of the sensitive area and that of the substrate. However, the buried legs must not interfere with the increased absorption provided by the resonant optical cavity.

6.2.2.2 CMOS ROIC

Honeywell employed a bipolar transistor as its pixel switch. Horizontal and vertical pixel addressing circuitry was integrated with the array but most of the analog readout circuitry was off-chip. Because of the lack of availability of A/D converters having sufficient speed (inverse of cycle time) with 14-bit accuracy, the array was segmented into 14 column groups with 14 parallel outputs.

Most of the approaches today employ CMOS silicon circuitry for which the power dissipation is much less than that of bipolar. More of the readout electronics has been moved onto the chip, where it is referred to as the readout integrated circuit (ROIC). The ROIC incorporates parallel column circuitry, consisting of amplifiers, integrators and sample-and-hold circuits with a column multiplexer which provides a single channel output.[5,6] With the improved A/D converters now available, only one is needed. It is usually off-chip but efforts are under way to move it on-chip.

6.2.2.3 Smaller pixels

Honeywell employed 50 × 50-μm pixels. It is desirable to reduce the pixel size in order to reduce the cost of the optics. (For a given *f*/no., on which the NETD depends, the cost of the optics made of Ge, the standard material, depends approximately upon the square of the diameter.) However, the NETD is inversely proportional to the pixel area, see Eq. (1.6). Thus, if the pixel size were reduced to 25 × 25 μm, and everything else remained the same, the NETD would increase

by a factor of four. Improvements in the readout electronics are needed to compensate for this. A 240 × 320 pixel array with 25-μm pixels having an NETD of 0.052 K (52 mK) is under development.[7]

6.2.2.4 640 × 480 pixel arrays

The development of a 640 × 480 pixel array employing 25 × 28-μm pixels is under way.[8] A focal plane array has been built and tested. The NETD is 0.113 K.

6.2.2.5 160 × 120 pixel arrays

Thermal imagers with 160 × 120 pixel arrays with 50 × 50-μm VOx pixels have been developed[9,10] with NETD values <0.1 K. The principal advantage of these smaller arrays over 320 × 240 arrays is cost reduction. More than four times as many small arrays can be obtained from one processed silicon wafer; the yield is higher and the off-chip electronics are simpler. In addition, the imagers require less electrical power and have smaller optics.

6.2.2.6 Removal of temperature stabilizer

The original Honeywell VOx bolometer array incorporated a thermoelectric temperature stabilizer to simplify the problem of pixel nonuniformity correction. However, the stabilizer consumes power and adds weight. Therefore, for some applications, such as that of unattended ground sensors, it is desirable to remove the temperature stabilizer. This has been achieved by calibration of each pixel over the expected range of ambient temperature.[11]

6.2.3 Use of amorphous silicon rather than vanadium oxide as the resistive material

Section 4.5.2 of Chapter 4 described the properties of amorphous hydrogenated silicon (a-Si:H) as a substitute for VOx in uncooled focal plane arrays. The presumed advantage of amorphous silicon is that its resistivity is sufficiently high that it can be continuously biased, rather than pulse biased, without excessive Joulean heating of the focal plane array.

Progress in the development of amorphous hydrogenated silicon uncooled focal plane arrays in the U.S.[12] and in France[13,14] has been reported. Amorphous hydrogenated silicon has a metastable state caused by defects arising from prolonged illumination. This is an undesirable feature that requires a specific annealing cycle during preparation. If not removed, it adversely affects long-term reliability.[14] Nevertheless, 320 × 240 uncooled arrays have been developed with an average NETD of 0.070 K.

6.2.4 Use of diodes rather than resistive materials

Instead of a resistive material as the temperature sensing element, Ishikawa et al.[15] have investigated the use of p-n junction diodes fabricated on silicon-on-insulator (SOI) substrates. The temperature dependence of the forward characteristic of the diode is measured. Rather than a microbridge structure, an absorbing film over the diode is employed. A 320 × 240 array using 40 × 40-μm pixels has been constructed. The NETD is reported to be 0.2 K.

6.2.5 Thermal imagers employing uncooled VOx bolometer arrays

Examples of thermal imagers employing 320 × 240 pixel VOx bolometer arrays now being marketed are Raytheon's AE-189[7] and Sanders Lockheed Martin's (now British Aerospace) LTC500.[16] Table 6-2 lists the performance parameters of the AE-189. Table 6-3 lists the performance parameters of the LTC500. These have been chosen as examples of derivatives of the original Honeywell work and not as product recommendations.

Boeing is marketing packaged 320 × 240 pixel VOx bolometer arrays (the product name of which is the V3000[17]) and is developing the V4000.[18] Thermal imagers employing 160 × 120 pixel VOx bolometer arrays have been developed[19,20] and are entering the marketplace. Again, these are not product recommendations. This is a rapidly evolving technology and market in which uncooled bolometric thermal imagers from worldwide suppliers are emerging.

6.2.6 Imaging radiometers based on 320 × 240 pixel uncooled VOx bolometers

An imaging radiometer is an imager with the additional capability of measuring the temperature of any point of a scene. It finds applications in the commercial and industrial world, principally in predictive and preventive maintenance and in process control.

Until the advent of uncooled imagers, imaging radiometers largely employed cryogenic focal plane arrays such as (Hg,Cd)Te (mercury cadmium telluride) and InSb (indium antimonide). With the advent of uncooled bolometer arrays and imagers, uncooled imaging radiometers have been developed. Because of the requirement for a large, linear dynamic temperature range, hybrid pyroelectric or hybrid ferroelectric bolometer arrays may be unsuitable for imaging radiometers. Uncooled thermoelectric arrays are suitable, and their application to imaging radiometers is discussed later in this chapter.

Table 6-2. Summary of performance characteristics of AE-189 microbolometer FPA. From W. Radford et al.[7]

Performance Parameter	Capability (*f*/1.0 and 300 K Scene)
Array configuration	320×240
Pixel size	50×50 μm
Overall chip dimensions	18.1×17.1 mm
Spectral response	8–14 μm
Signal responsivity	$> 5 \times 10^6$ V/W or 10 mV/K_{scene}
NETD @ *f*/1	< 100 mK
Output offset nonuniformity	< 300 mVp-p
Output noise	1.0 mV RMS
Intrascene dynamic range @ *f*/1	> 200 K
Uncorrected responsivity nonuniformity	< 4% (sigma/mean)
Pixel operability	> 99.5%
Crosstalk (nearest neighbor)	< 1% (combined optical and electrical)
Power dissipation	75 mW
Nominal operating temperature	20°C

Table 6-3. Sanders Lockheed Martin LTC500 thermal imager technical specifications. From T. Breen et al.[16]

LTC500 Camera Technical Specifications	
Standard imaging module	SIM100
Spectral response	8–14 μm
Available horizontal FOV	4.3°–50.6°
IFOV for 5.6° system	0.3 mrad
Video output	RS-170/NTSC or PAL
Digital output options	15 bit real time
Array format	327×245
NETD (*f*/1, 30 Hz)	< 100 mK
Frame update rate	60 Hz
Size (including 40° lens)	4.5 in. (H) × 5.0 in. (W) × 12.6 in. (L)
Weight (including 40° lens)	5.5 pounds
Power	4-29 V DC, < 10 W

Uncooled imaging radiometers employing resistive bolometer arrays are basically uncooled imagers that have calibrated pixels, the calibration coefficients having been stored in memory and stored algorithms employed with a microprocessor to calculate temperature by means of the output signal from each pixel. The calibrations must provide a continuous curve of the output voltage of every pixel as a function of temperature from a standard blackbody over a wide dynamic range. Furthermore, each of these pixel calibrations must be in terms of the ambient temperature of each pixel over a range of ambient temperatures. A description is provided by Meyer and Hoelter.[21] The present technology is based on 320 × 240 VOx arrays.

6.2.7 Summary

The de facto standard resistive microbolometer array, a derivative of the original Honeywell array, has the following features:

- Silicon microstructure
- VOx resistive material
- 50 × 50-μm pixels
- Response time of 12 msec
- 30-Hz frame rate
- 8–14 μm spectral response
- NETD of 0.05 K (blackbody temperature = 300 K, frame rate = 30 Hz, *f*/1 optics)

These arrays are employed in commercially available uncooled thermal imagers and imaging radiometers.

VOx uncooled thermal imagers employing 160 × 120, 50 × 50-μm pixels with NETD < 0.1 K (blackbody temperature = 300 K, frame rate = 30 Hz, *f*/1 optics) are becoming available commercially.

Under development are 640 × 480 pixel arrays having 28 × 28-μm pixels. The NETD of 0.113 K is expected to improve substantially.

Alternative materials, especially hydrogenated amorphous silicon, are candidates to replace VOx.

6.3 Pyroelectric and Ferroelectric Bolometer Uncooled Arrays and Thermal Imagers that Employ Them

6.3.1 Introduction

The worldwide development of pyroelectric and ferroelectric bolometer arrays stems principally from efforts at two corporations, namely, Texas Instruments (now Raytheon) in the U.S. and GEC Marconi (now British Aerospace) in the United Kingdom. The U.S. effort, funded by DARPA and U.S. Army CECOM

NVESD, which was the larger effort, will be the principal subject of this discussion.

6.3.2 The Texas Instruments (now Raytheon) hybrid ferroelectric bolometer array and imagers

In contrast to the Honeywell effort that employed a silicon microstructure for thermal isolation, the Texas Instruments effort employed a hybrid structure. In this approach, a silicon substrate with embedded electronics at each pixel was prepared separately from the detecting material, which was then bump-bonded to the substrate at each pixel. The detecting material was barium strontium titanate, a ceramic whose ferroelectric properties, including the Curie temperature, could be adjusted by the barium-to-strontium ratio. Rather than operating as a pyroelectric detector, this focal plane array was operated as a ferroelectric bolometer, also known as a bias-enhanced pyroelectric detector. Like the Honeywell resistive bolometer development, the Texas Instruments ferroelectric bolometer development was an outstanding success. On the other hand, the hybrid structure (in which the thermal isolation capability is limited by the thermal conductance of the bump bonds) has limited the potential for performance improvement, especially a better (lower) NETD.

The description of the pyroelectric effect in Chapter 5 did not include electrical bias enhancement. The reasons are twofold: the subject is extremely complex, and future developments will most likely be limited to pyroelectric detectors without bias enhancement on silicon microstructure substrates. The best source of information on the hybrid ferroelectric bolometer is the chapter by Hanson[22] who led the Texas Instruments ferroelectric bolometer development. Like the Honeywell resistive bolometer development, that effort was classified until mid-year 1992. A brief description of the operation is presented here.

In contrast to the pyroelectric effect on silicon microstructures, in which the Curie temperature is far above the operating temperature of the pyroelectric effect, the hybrid ferroelectric effect is stabilized at a temperature just below the Curie temperature. (Recall that the Curie temperature is the temperature above which a material loses its ferroelectric properties). As Fig. 6-6 shows, the slope of the ferroelectric polarization versus temperature is highest at that point. (Recall that the ferroelectric polarization is the electric dipole moment per unit volume of material; the pyroelectric coefficient is the slope of the polarization versus temperature curve at the operating temperature; and the pyroelectric current is proportional to the pyroelectric coefficient and the rate of change of temperature with respect to time.)

Consider now the dependence of the dielectric permittivity with temperature on either side of the Curie temperature. The pyroelectric pixel is a capacitor; like all capacitors, its capacitance depends on its dielectric constant or relative permittivity. Figure 6-7 shows that near the Curie temperature, the relative permittivity changes rapidly with temperature. If only the change in relative

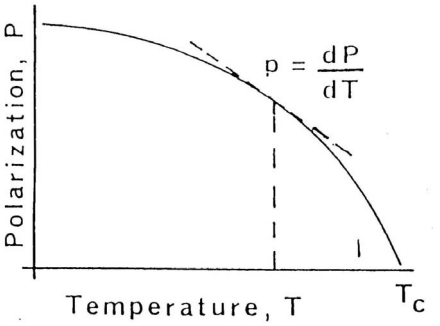

$$i_s = pA\frac{dT}{dt}$$

P = Polarization = electric dipole moment per unit volume of material (Coul/cm^2)
Electric dipole moment = surface charge multiplied by average distance between positive and negative charges (Coul cm)

p = Pyroelectric coefficient (Coul/cm^2 °C)

T = Temperature (°C)

T_c = Curie temperature (°C)

t = Time (sec)

A = Area of pyroelectric sample (cm^2)

Figure 6-6. The pyroelectric effect.

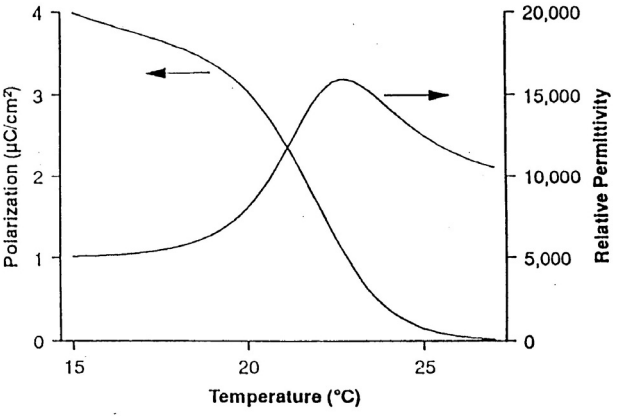

Figure 6-7. Temperature dependence of spontaneous polarization and dielectric permittivity for ferroelectric ceramic barium strontium titanate (BST). From C. M. Hanson et al.[23]

permittivity with temperature is monitored, which can only be done by means of an electrical bias, the device is termed a "dielectric bolometer." Operation in this mode has been explored by Noda et al.[24] On the other hand, if simultaneous operation in both the pyroelectric and dielectric bolometer modes is employed, the detector is referred to as a "ferroelectric bolometer" or a "bias-enhanced" pyroelectric detector. Figure 6-8 illustrates the dependence of responsivity on temperature and applied voltage of a Texas Instruments barium strontium titanate ferroelectric bolometer.

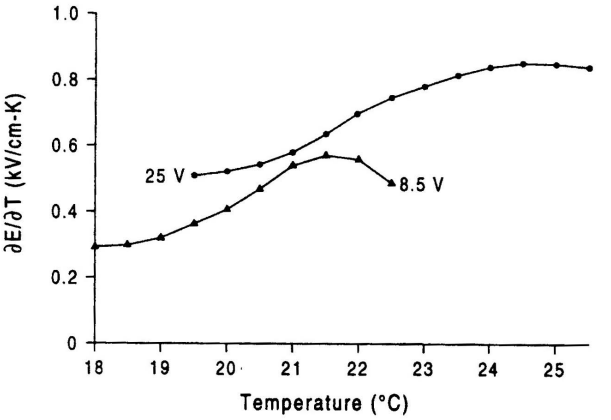

Figure 6-8. Pyroelectric material responsivity figure of merit $[\partial E/\partial T)_D = p/\varepsilon\varepsilon_o]$ for a ceramic $Ba_{0.67}Sr_{0.33}TiO_3$ (barium strontium titanate) sample 25-μm thick, at two different bias voltages. From C. M. Hanson.[23]

The construction and performance of the Texas Instruments hybrid ferroelectric bolometer array has also been described by several authors.[25,26] Figure 6-9 shows the construction of the array. Under each pixel is the readout integrated circuit (ROIC) illustrated in Fig. 6-10. As pointed out in Eq. (5.16), there is both a thermal and an electrical time constant for a pyroelectric detector. The combination of these with the ROIC effectively limits the noise (and signal) of the Texas Instruments hybrid ferroelectric bolometer from about 1 Hz to about 200 Hz. Of course, there is no dc signal; a radiation chopper must be employed.

How well did the Texas Instruments ferroelectric bolometer operate when declassified in 1992? The best NETD measured was about 0.04°C for a 300 K blackbody and *f*/1 optics, essentially the same as that of the Honeywell resistive bolometer. How can this be, since the Honeywell monolithic resistive bolometer has superior thermal isolation compared with the Texas Instruments hybrid ferroelectric bolometer? The reason is that the Texas Instruments device is almost temperature fluctuation noise limited whereas the Honeywell one is not. Referring to Eq. (2.29), it can be seen that for a Texas Instruments thermal conductance G of about 2×10^{-6} W/deg K, the 300 K temperature fluctuation noise limit is about 0.020 K, whereas for a Honeywell G value of about 1×10^{-7} W/deg

K, the temperature fluctuation noise limit is about 0.005 K. In other words, excess electrical noise in the wider electrical bandwidth (compared with Texas Instruments) and a responsivity limited by the Joulean heating of the pixels by the bias current prevented the Honeywell device from being at the temperature fluctuation noise limit.

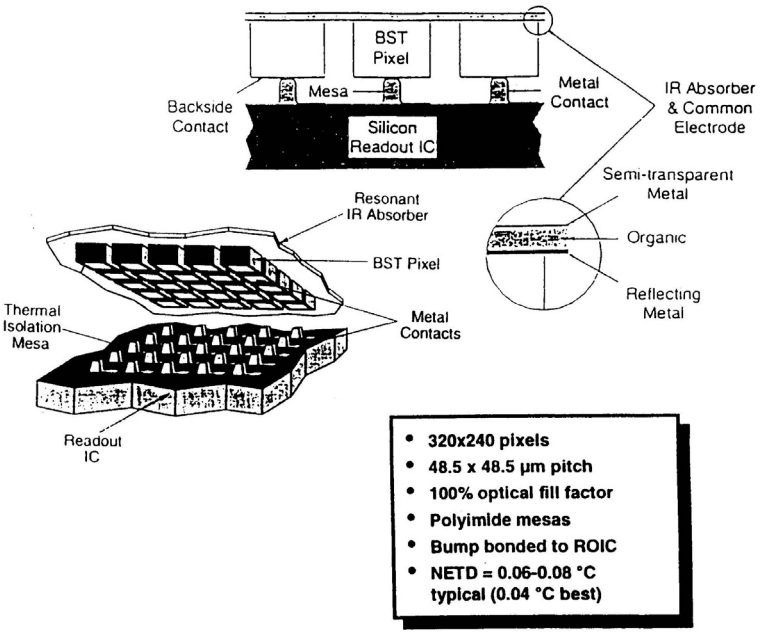

Figure 6-9. The Texas Instruments (now Raytheon) hybrid ferroelectric bolometer array. From C. M. Hanson et al.[23]

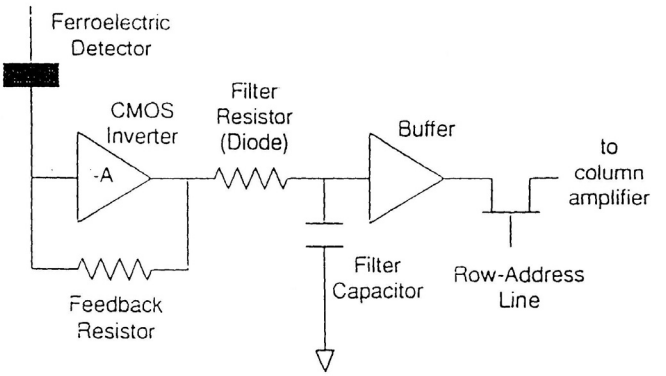

Figure 6-10. Read-out integrated circuit for Texas Instruments (now Raytheon) hybrid ferroelectric array. From C. M. Hanson et al.[23]

Even though the hybrid design limits the performance of the Texas Instruments (now Raytheon) ferroelectric bolometer, its performance is good enough for many applications. These include use by the police, by firefighters, for drivers' vision enhancement and many others. Currently it is more widely used than resistive bolometer systems, although this will probably change in the near future.

6.3.3 Monolithic pyroelectric array development

Because the hybrid design is difficult to improve, Raytheon[27] and British Aerospace[28] are developing monolithic pyroelectric arrays (see Fig. 6-11). These devices are in early development; whether they will be competitive in performance and cost with the monolithic resistive bolometer arrays remains to be seen. Their need for a radiation chopper may limit their use in some applications.

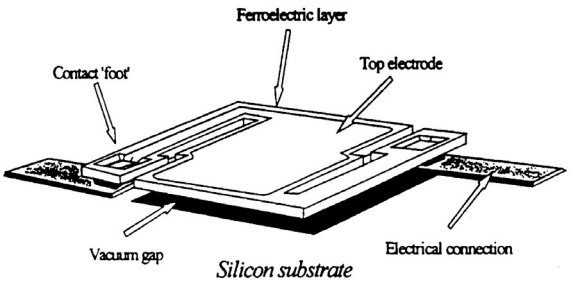

Figure 6-11. Silicon microstructure monolithic pyroelectric array. From R. K. McEwen and P. A. Manning.[28]

6.4 Uncooled Thermoelectric Arrays and Thermal Imagers and Imaging Radiometers that Employ Them

6.4.1 Introduction

Although uncooled thermoelectric arrays can have D* values comparable to uncooled pyroelectric, ferroelectric bolometer, and resistive bolometer arrays, much less effort has been made in their development. The reason is that their responsivity (and also their noise) is orders of magnitude less. Thus their application in thermal imaging systems requires very low-noise electronics to realize their performance potential. Because the signal-to-noise ratio is a function of system bandwidth, which is directly related to imager frame rate, they have found almost no use as matrix arrays in TV frame rate imagers. Instead, they are

employed as linear arrays that are mechanically scanned to form an image of stationary or nearly stationary objects. Their inherent linearity with incident radiant power, and their very large dynamic range, are attractive features for industrial radiometry, such as in predictive and preventive maintenance. They also find application in space systems such as horizon scanners and planetary imagers where their unbiased operation minimizes system power drain.

The state of the art of thermoelectric arrays and their applications is discussed below, as reflected by the scientific and engineering literature. The first example is that of high performance monolithic linear arrays. That is followed by a description of an imaging radiometer employing a linear array.

6.4.2 Monolithic linear arrays

Foote and colleagues[29] have described the preparation and performance of bismuth tellurium (Bi-Te) and bismuth antimony tellurium (Bi-Sb-Te) monolithic linear arrays of several geometrics. Common to all is the use of a silicon nitride membrane over a cavity in a silicon substrate. Table 6-4, from Foote and Jones,[30] lists the parameters of four types of arrays shown in Figs. 6-12(a) through (d) which differ in pixel size and number of thermocouples per pixel. Compared with most other thermoelectric arrays, their D* values are exceptionally high. Figure 6-13, from Foote and Jones,[30] compares the performance of their arrays with 12 others reported in the literature.

Table 6-4. Geometry and measured performance of four thermopile arrays shown in Figs. 6-12(a) through (d). From M.C. Foote and E.W. Jones.[30]

Parameter	Device Type 1	Device Type 2	Device Type 3	Device Type 4
Detector length (μm)	1,500	184	176	70
Pixel pitch (μm)	75	104	104	54
Number of thermocouples per pixel	11	1	5	1
Number of devices tested	126	21	31	19
Resistance (Ω)	40,000	2,900	12,000	1,650
dc infrared responsivity (V/W)	1,100	1,120	1,060	866
Response time (ms)	99	83	23	15
D* (1000 K, 0 Hz) (10^8 cm $Hz^{1/2}$/W)	14	22	9.8	9.7

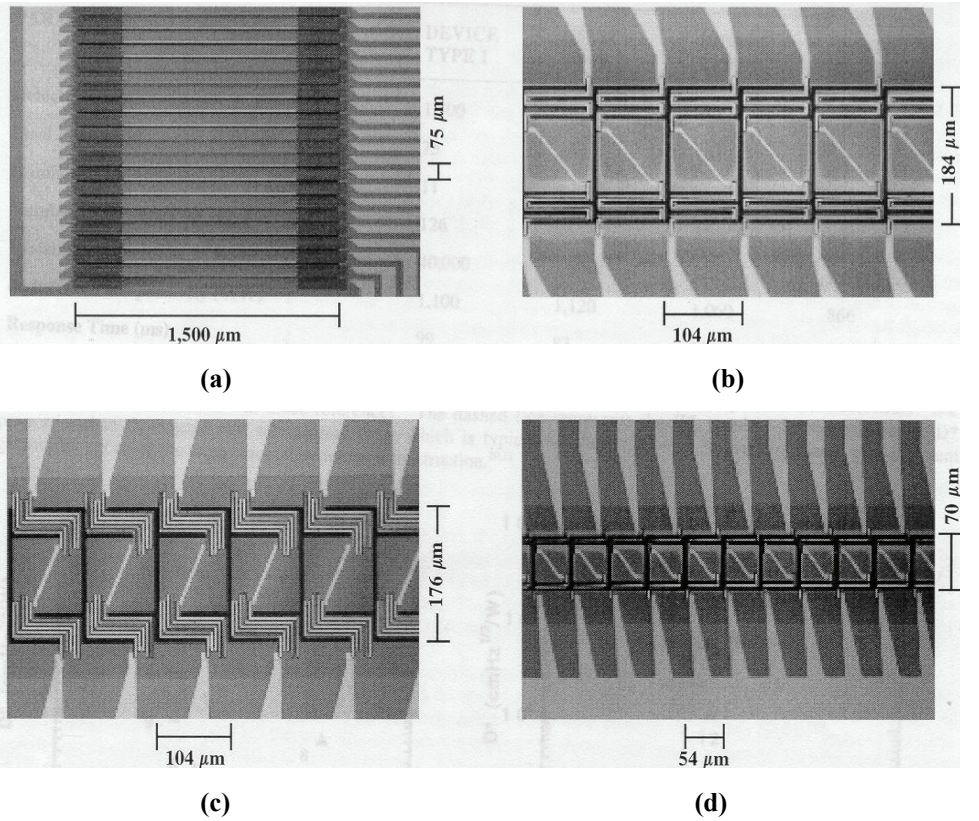

Figure 6-12. Four types of uncooled thermopile arrays: (a) Array of type 1 thermopile devices. The 0.6-μm thick device membranes connect to the silicon substrate at the left and right sides. Each pixel has 11 Bi-Te/Bi-Sb-Te thermocouples in series. These long, thin devices were designed to geometrically match a spectrometer. (b) Array of type 2 thermopile devices. The 0.6-μm thick device membranes connect to the silicon substrate at the top and bottom. Each pixel has one Bi-Te/Bi-Sb-Te thermocouple. (c) Array of type 3 thermopile devices. The 0.6-μm thick device membranes connect to the silicon substrates at the top and bottom. Each pixel has five Bi-Te/Bi-Sb-Te thermocouples in series. (d) Array of type 4 thermopile devices. The 0.6-μm thick device membranes connect to the silicon substrate at the top and bottom. Each pixel has one Bi-Te/Bi-Sb-Te thermocouple. From M.C. Foote and E.W. Jones.[30] Provided through the courtesy of the Jet Propulsion Laboratory, California Institute of Technology, Pasadena, California.

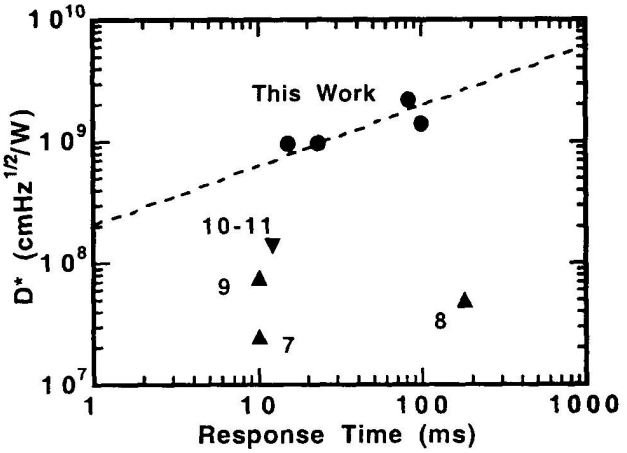

Figure 6-13. Representative data from the literature showing reported D* values as a function of response time for thin film thermopile linear arrays. Thermoelectric materials are Bi-Te/Bi-Sb-Te (this work) (ℓ), constantan/chromel (↔), and silicon (↔). The dashed line represents the Foote and Jones results. Its slope indicates D* proportional to the square root of response time, which is typical for thermopiles or bolometers with different geometries and the same material system. From M.C. Foote and E.W. Jones.[30] See Foote and Jones[30] for identification of the numbered data points. Provided through the courtesy of the Jet Propulsion Laboratory, California Institute of Technology, Pasadena, California.

6.4.3 Imaging radiometer employing linear thermoelectric arrays

McManus and Mickelson[31] and Kruse[32] have described the construction, performance, and applications of an imaging radiometer that employs a 120-pixel linear array of chromel-constantan thermopiles, each thermopile consisting of three series-connected thermocouples with a pitch of 50 μm (see Table 6-5). These thin-film thermocouples are deposited on a silicon nitride membrane over an etch pit in a silicon substrate (see Fig. 3-2). To provide a thermal image of a scene, a stepper motor drives the vertically oriented linear array across the focal plane of a germanium lens in 1.4 s. The resultant image, displayed in false colors, representing temperature variation, on a color liquid crystal display, contains 120 × 120 pixels. A cursor is employed to read out the temperature at any point of the image. A removable PCMCIA memory card stores 144 images for recall and later transfer to a computer. An RS-232 port provides an interface to a personal computer. Operation is controlled by a built-in 386EX microprocessor. The specifications are listed in Table 6-6. (Description of this imaging radiometer is not meant to be a product recommendation.)

Table 6-5. Specifications of thermoelectric linear arrays employed in IR SnapShot® imaging radiometer. From P.W. Kruse.[32]

Number of pixels	128
Number of pixels accessed	120
Pixel size (μm)	50
Number of junctions per pixel	3
Resistance at 300 K (Ohms)	2,380
Thermal response time (msec)	12
Responsivity (V/W)	265
D* (cm $Hz^{1/2}$/W)	1.7×10^8

Table 6-6. IR SnapShot® imaging radiometer specifications.

Detector	120 element linear array of uncooled thermoelectric detectors, 50-μm square pixels
System dynamic range	12 bits usable with digitizing resolution of 16 bits
Field of view	17.2 deg horizontal and 17.2 deg vertical
Lens	germanium 20 mm, F/0.8
Spectral band	8 to 12 μm
NETD	<0.1°C @ 30°C
Accuracy	2°C or 2% of reading
Measurement temperature range	0 to 350°C (custom range available)
Operating temperature	0 to 40°C
Power input	camcorder battery
Image scan time	<1.5 s
Battery operating time	>60 min. with 3 AH battery
Image storage	144 images
Communication	RS-232
Display	active matrix color LCD
Video output	selectable NTSC/PAL
Setup menu options	emissivity, background temperature, temperature units, color palette, autoscale and fixed ranges, focus width, time, date, RS-232 baud rate, NTSC/PAL select
Size	$9.4 \times 3.9 \times 5.1$ in., not including lens
Weight	4.4 lbs with lens and battery

6.5 Status and Trends of Uncooled Arrays

This section presents the status and technical trends of uncooled arrays, divided between those in production and under development for military and for commercial applications.

6.5.1 Status and trends of uncooled arrays for military systems

Table 6-7 illustrates the status and trends of uncooled arrays for military applications. Both resistive bolometers and ferroelectric bolometers are employed today for uncooled thermal imaging military systems. The arrays have 320 × 240 pixels, each 50-μm square. The NETD requirement, which is being met, is 0.1°C. The frame rate is 30 Hz in the U.S.

Table 6-7. Status and trends of military uncooled arrays.

Military Requirements Emphasize High Performance

Status	Trends
Resistive bolometer, ferroelectric bolometer	Resistive bolometer
320 × 240 pixels	640 × 480 pixels
	160 × 120 pixels
0.1°C NETD	0.01°C NETD
50 × 50-μm pixel size	35 × 35-μm pixel size
	25 × 25-μm pixel size
30-Hz frame rate	30-Hz frame rate

Under development are resistive bolometer arrays containing 640 × 480 pixels. The pixel size is being reduced to 25 × 25 μm; 35 × 35 μm is an intermediate objective. The NETD goal is 0.01°C for high performance applications. Lower cost/lower performance applications, such as fieldable perimeter security sensors, use 160 × 120 pixels, 50 × 50 μm, and an NETD of 0.1°C. The frame rate remains 30 Hz in the U.S.

Because the NETD depends inversely on the pixel sensitive area, it will be difficult to reduce both the pixel size and the NETD in the same array. The 640 × 480 pixel arrays will use small pixels, i.e., less than 50 × 50 μm, in order to reduce the optics cost. Thus the NETD of these larger arrays will remain at 0.1°C for the near future.

6.5.2 Status and trends of commercial uncooled arrays and systems

Table 6-8 illustrates the status and trends of uncooled arrays for commercial applications. The systems in use today including resistive bolometer imagers and imaging radiometers and ferroelectric bolometer imagers are derivatives of military systems and are too costly for widespread use. Imaging radiometers employing linear thermoelectric arrays operating in the snapshot mode are less costly than the TV-rate imaging radiometers employing resistive bolometer arrays.

As the commercial markets for uncooled imagers and imaging radiometers expand, and as the military environmental requirements are replaced by commercial requirements that are easier to meet, the cost of commercial systems will inevitably decrease. If the drivers' vision enhancement system market undergoes explosive growth, as appears possible, thermal imager costs will dramatically decrease.

Table 6-8. Status and trends of commercial uncooled arrays.

Commercial Markets Emphasize Low Cost*

Status	Trend
Commercial marketing of military thermal imagers	Development of new, low-cost thermal imagers and imaging radiometers
Overspecified for commercial applications	Designed for specific commercial applications and meeting commercial requirements
320×240 pixel, 50×50 μm, bolometer arrays for thermal imagers that cost \$15,000–\$20,000, and imaging radiometers that cost \$20,000–\$50,000	160×120 pixel, 50×50 μm, bolometer arrays for thermal imagers which cost < \$3,000, imaging radiometers that cost < \$5,000, and drivers' vision enhancement systems that cost < \$2,000
120×1 pixel, 50×50 μm, thermoelectric arrays for imaging radiometers that cost \$15,000	Same performance but cost \$7,500
320×240 pixel, 50×50 μm, hybrid ferroelectric bolometer array imagers for drivers' vision enhancement that cost \$2,000–\$4,000 in extremely large volumes	160×120 pixel, 50×50 μm, bolometer arrays for drivers' vision enhancement that cost \$1,000 in extremely large volumes

*The term "cost" refers to what the buyer pays.

References

1. P.W. Kruse, L.D. McGlauchlin and R.B. McQuistan, *Elements of Infrared Technology*, Chapter 9, John Wiley and Sons, New York, (1962).
2. R.A. Wood, C.J. Han, and P.W. Kruse, "Integrated uncooled infrared detector imaging array," Proc. IEEE Solid State Sensor and Actuator Workshop, Hilton Head Island, SC, pp. 132-135 (1992).
3. R.A. Wood, "Monolithic silicon microbolometer arrays," in *Uncooled Infrared Imaging Arrays and Systems*, Vol. 47 of *Semiconductors and Semimetals*, P.W. Kruse and D.D. Skatrud, eds., Academic Press, New York (1997).
4. R.S. Balcerak, "Uncooled infrared sensors: rapid growth and future perspective," Proc. SPIE Vol. 4028, *Infrared Detectors and Focal Plane Arrays VI*, p. 36 (2000).
5. P.E. Howard et al., "Advances in microbolometer focal plane array technology at Boeing," Proc. SPIE Vol. 3379, *Infrared Detectors and Focal Plane Arrays V*, p. 47 (1998).
6. P.E. Howard et al., "Advanced high-performance 320×240 VOx microbolometer uncooled IR focal plane," Proc. SPIE Vol. 3698, *Infrared Technology and Applications XXV*, p. 131 (1999).
7. W. Radford et al., "Sensitivity improvements in uncooled microbolometer FPAs," Proc. SPIE Vol. 3698, *Infrared Technology and Applications XXV*, p. 119 (1999).
8. R. Murphy et al., "Recent developments in uncooled IR technology," Proc. SPIE Vol. 4028, *Infrared Detectors and Focal Plane Arrays VI*, p. 12 (2000).
9. P.W. Kruse et al., "Infrared imager employing 160×120 pixel uncooled bolometer array," Proc. SPIE Vol. 3436, *Infrared Technology and Applications XXIV*, p. 572 (1998).
10. J.L. Heath et al., "160×128 uncooled FPA performance review," Proc. SPIE Vol. 3698, *Infrared Technology and Applications XXV*, p. 256 (1999).
11. Personal communication from Infrared Solutions, Inc.
12. J.F. Brady et al., "Advances in amorphous silicon uncooled IR systems," Proc. SPIE Vol. 3698, *Infrared Technology and Applications XXV*, p. 161 (1999).
13. C. Vedel et al., "Amorphous-silicon-based uncooled microbolometer IRFPA," Proc. SPIE Vol. 3698, *Infrared Technology and Applications XXV*, p. 276 (1999).
14. E. Mottin et al., "320×240 microbolometer uncooled IRFPA," Proc. SPIE Vol. 4028, *Infrared Detectors and Focal Plane Arrays VI*, p. 40 (2000).
15. T. Ishikawa et al., "Low cost 320×240 uncooled IRFPA using conventional silicon IC process," Proc. SPIE Vol. 3698, *Infrared Technology and Applications XXV*, p. 556 (1999).

16. T. Breen et al., "Applications of uncooled microbolometer sensors," Proc. SPIE Vol. 3379, *Infrared Detectors and Focal Plane Arrays V*, p. 145 (1998).
17. P.E. Howard, "Advances in microbolometer focal plane technology at Boeing," Proc. SPIE Vol. 3379, *Infrared Detectors and Focal Plane Arrays V*, p. 47 (1998).
18. P.E. Howard et al., "Advanced high-performance 320×240 VOx microbolometer uncooled IR focal plane array," Proc. SPIE Vol. 3698, *Infrared Technology and Applications XXV*, p. 131 (1999).
19. P.W. Kruse et al., "Infrared imager employing 160×120 pixel uncooled bolometer array," Proc. SPIE Vol. 3436, *Infrared Technology and Applications XXIV*, p. 572 (1998).
20. J.L. Heath et al., "160×128 uncooled FPA performance review," Proc. SPIE Vol. 3698, *Infrared Technology and Applications XXV*, p. 256 (1999).
21. B. Meyer and T. Hoelter, "Uncooled radiometric camera performance," Proc. SPIE Vol. 3379, *Infrared Detectors and Focal Plane Arrays V*, p. 69 (1998).
22. C. M. Hanson, "Hybrid pyroelectric-ferroelectric bolometer arrays," Chapter 4 in *Uncooled Infrared Imaging Arrays and Systems*, *Semiconductors and Semimetals 47*, Paul W. Kruse and David D. Skatrud, eds., Academic Press, New York (1997).
23. C.M. Hanson et al., Proc. SPIE Vol. 1735, p. 17 (1992).
24. M. Noda et al., "Simple detector pixel of dielectric bolometer mode and its device structure for an uncooled IR image sensor," Proc. SPIE Vol. 3698, *Infrared Technology and Applications XXV*, p. 565 (1999).
25. R. Owen et al., "Producibility advances in hybrid uncooled infrared devices-II," Proc. SPIE Vol. 2746, *Infrared Detectors and Focal Plane Arrays V*, p. 23 (1996).
26. S.B. Evans and T. Hayden, "High MTF hybrid ferroelectric IRFPA," Proc. SPIE Vol. 3379, *Infrared Detectors and Focal Plane Arrays V*, p. 36 (1998).
27. J.F. Belcher et al., "Uncooled monolithic ferroelectric IRFPA technology," Proc. SPIE Vol. 3436, *Infrared Technology and Applications XXIV*, p. 611 (1998).
28. R.K. McEwen and P.A. Manning, "European uncooled thermal imaging sensors," Proc. SPIE Vol. 3698, *Infrared Technology and Applications XXV*, p. 322 (1999).
29. M.C. Foote, E.W. Jones and T. Caillat, "Uncooled thermopile infrared detector linear arrays with detectivity greater than 10^9 cmHz$^{1/2}$/W," *IEEE Trans. Electron Dev*. **45**, p. 1896 (1998).
30. M.C. Foote and E.W. Jones, "High performance micromachined thermopile linear arrays," Proc. SPIE Vol. 3379, *Infrared Detectors and Focal Plane Arrays V*, p. 192 (1998).
31. T. McManus and S. Mickelson, "Imaging radiometers employing linear thermoelectric arrays," Proc. SPIE Vol. 3698, *Infrared Technology and Applications XXV*, (1999).

32. P. W. Kruse, "Application of uncooled monolithic thermoelectric linear arrays to imaging radiometers," in *Uncooled Infrared Imaging Arrays and Systems*, P. W. Kruse and D. D. Skatrud, eds., *Semiconductors and Semimetals 47*, R.K. Willardson and E.R. Weber, eds, Academic Press, San Diego (1997).